Nature Methods

Instant super-resolution imaging in live cells and embryos via analog image processing

Andrew G. York, Panagiotis Chandris, Damian Dalle Nogare, Jeffrey Head, Peter Wawrzusin, Robert S. Fischer, Ajay Chitnis, Hari Shroff

Supplementary Fig. 1, Instant SIM Optical Setup.

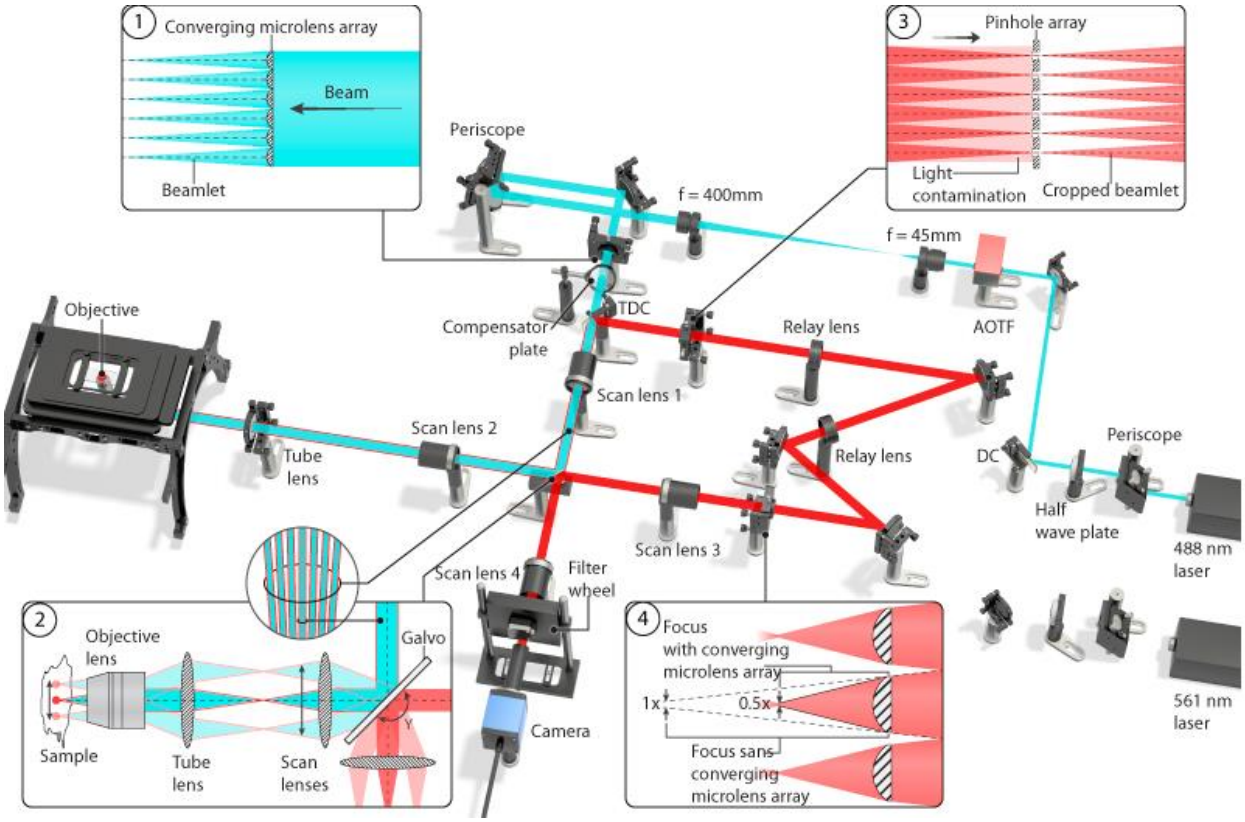

488 nm and 561 nm lasers are used to excite fluorescence from the sample. Lasers are combined with dichroic DC and passed through an AOTF (providing fast shuttering, and power control in conjunction with half-wave plates placed in front of each laser), beam expander, converging microlens array (to form a multiplicity of excitation foci, **inset 1**), compensator plate (to minimize astigmatism), thick dichroic TDC, scan lens telescope (Scan Lens 1 and 2) with galvanometric mirror (Galvo) placed between lenses (to scan the multifocal excitation array through the sample, thus covering the imaging field, **inset 2**), tube lens and objective. Multifocal fluorescence from sample is collected with the same objective and passed through tube lens, Scan lenses 1 and 2, Galvo, and reflected from TDC. In the descan path (post Galvo), fluorescence is stationary, so a pinhole array placed at the focal plane of Scan lens 1 serves to reject out of focus fluorescence (**inset 3**). Relaying the emission to a second microlens array is achieved by relay lenses; the second microlens array serves to locally contract each focus 2x, while maintaining the foci orientation (**inset 4** and **Supplementary Fig. 3**). The locally scaled foci are rescanned and imaged onto a sCMOS camera via Scan lens 3, the Galvo, and Scan lens 4; excitation light is removed by emission filters inside a Filter wheel placed immediately before the camera.

Supplementary Fig. 2, Brightfield imaging with instant SIM.

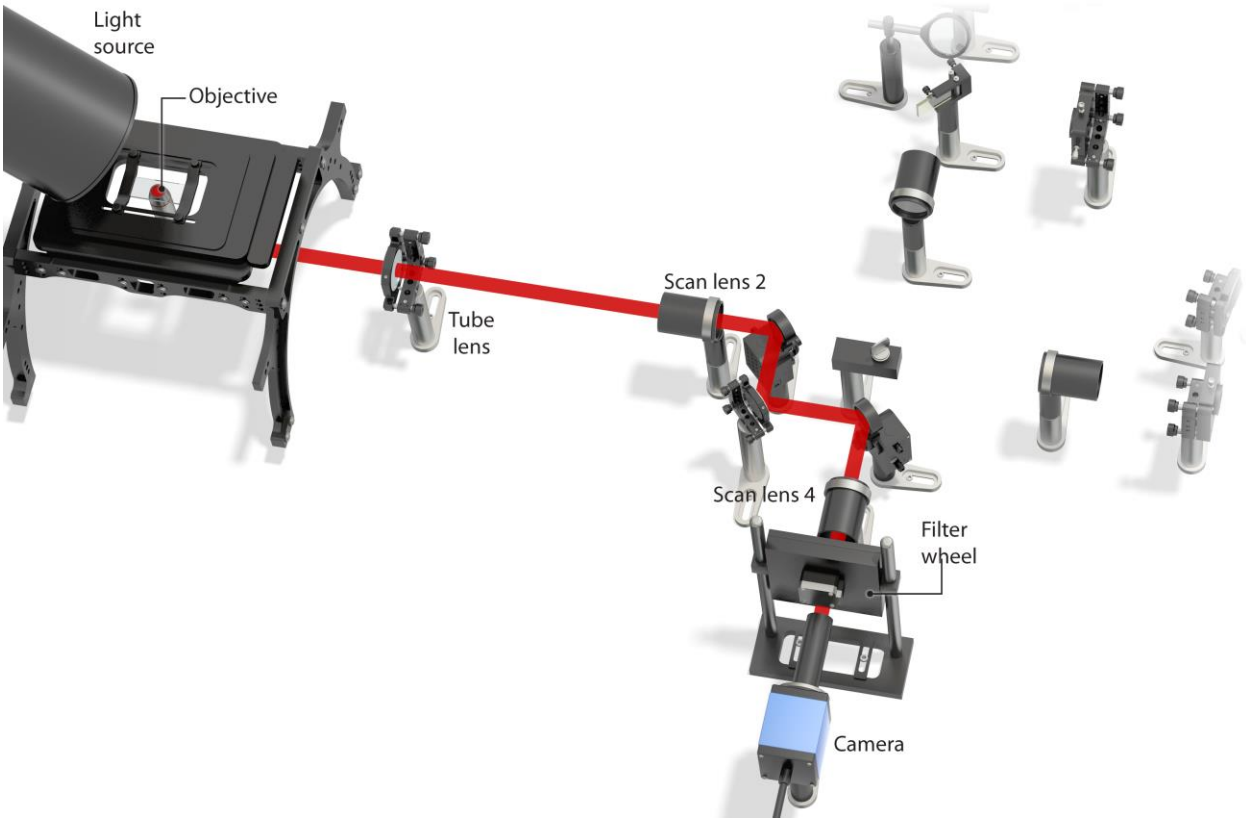

A lamp is used to illuminate the sample from above. Transmitted light is collected via the objective, passed through the Tube lens and Scan lens 2, and directed through Scan lens 4 via removable mirrors before imaging onto the camera.

Supplementary Fig. 3, Forming an upright image half the size of an object.

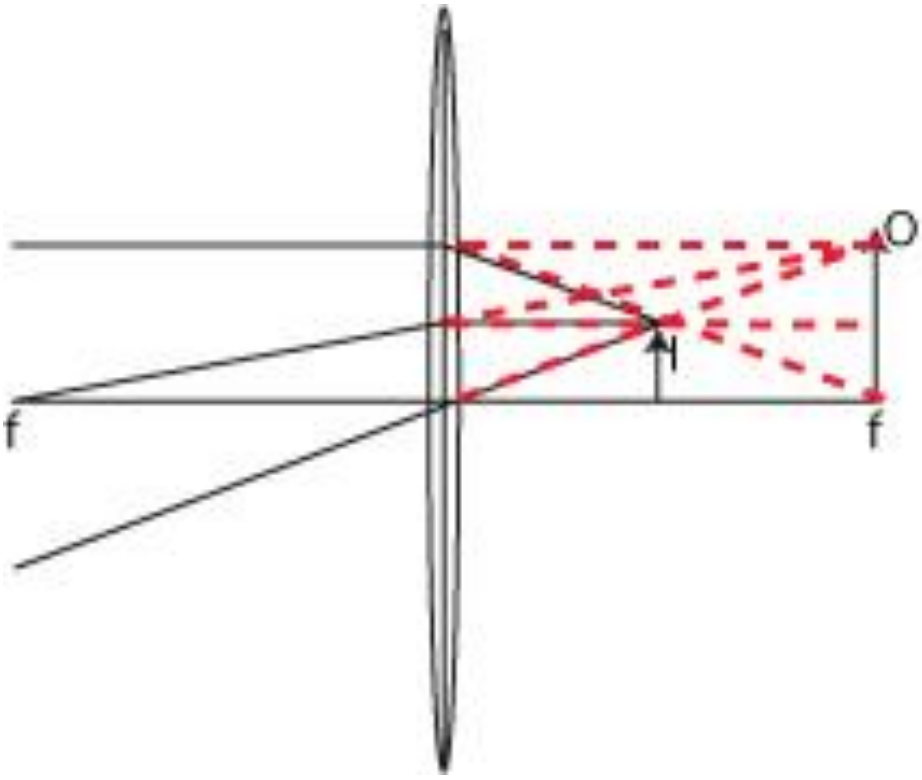

A virtual object (O) placed at the right-hand focal point (f) produces an upright image (I) one half the object size, located on the same side of the lens. Three rays were traced from the virtual object (red dotted lines, for clarity shown only on the right side of the lens): (1) a ray parallel to the optic axis is refracted through the lens and passes through the right focal point; (2) a ray en route to the left focal point emerges horizontal to the optic axis; (3) a ray that passes through the center point of the lens continues undeflected. The intersection of these rays at *f*/2 indicates the image position. Tracing the rays back through the lens (on its left side) indicates the real rays (black) that would have formed the object (if the lens had not been placed in the optical path); these real rays are refracted by the lens to form the image.

Supplementary Fig. 4, Example control voltages for 5-timepoint, 2-color timelapse 2D acquisition.

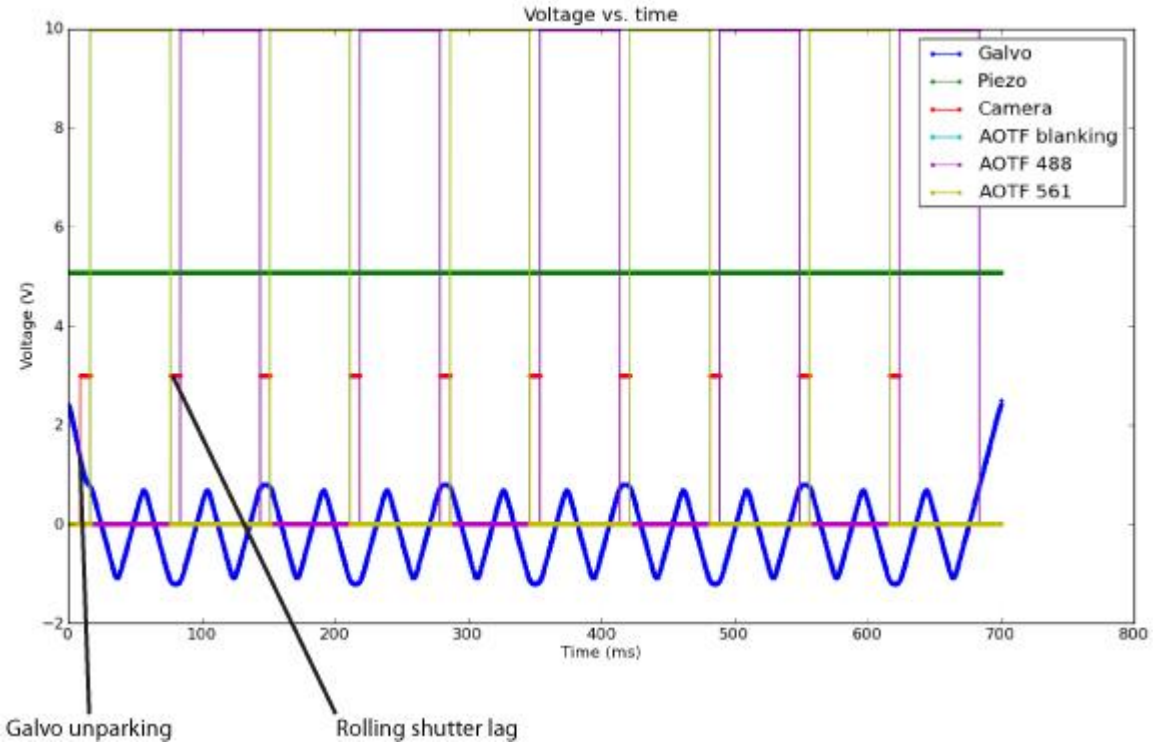

See online methods for accompanying description.

Supplementary Fig. 5, Example control voltages for a 4-slice, 2-color Z-stack.

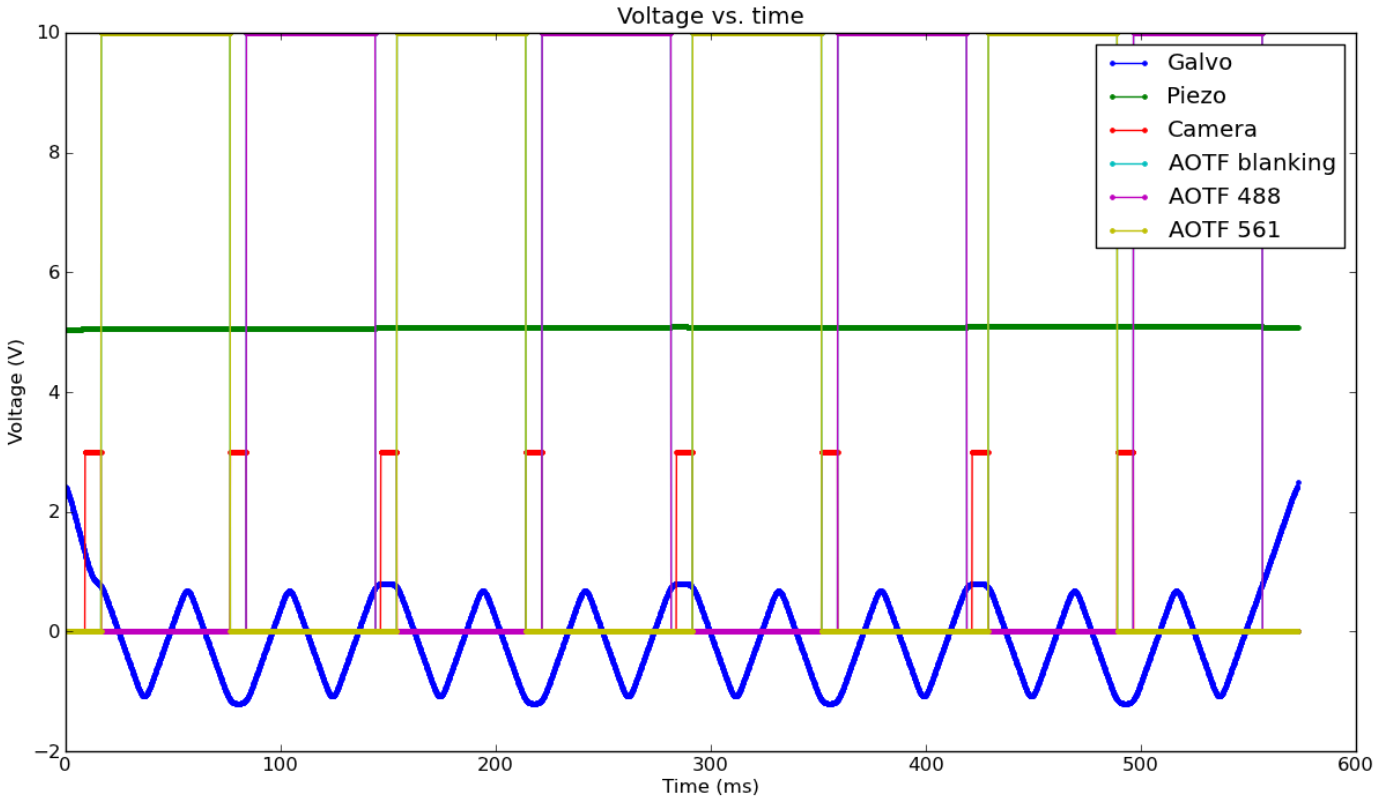

See online methods for accompanying description. See also higher magnification view in **Supplementary Fig. 6**.

Supplementary Fig. 6, Vibration control scheme for rapid Z axis piezo stage movement.

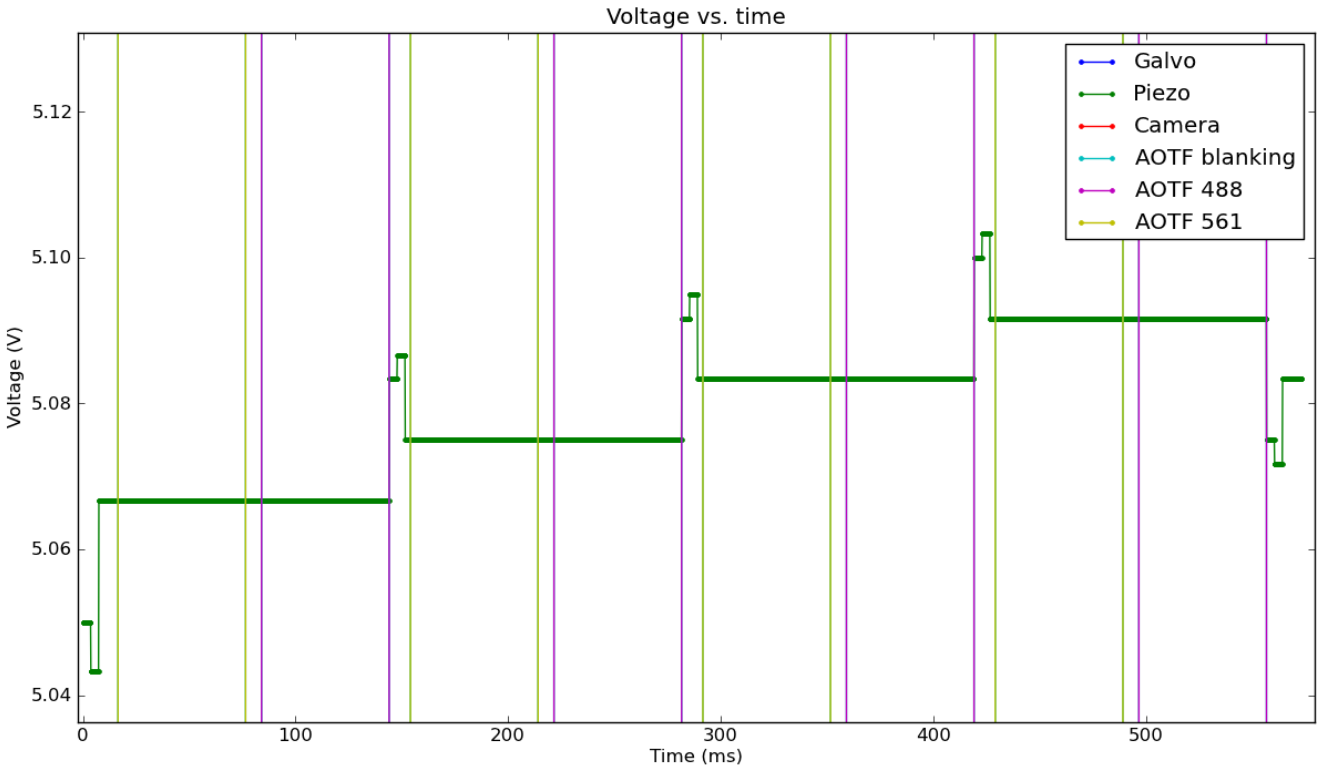

Higher magnification view of voltages in **Supplementary Fig. 5**, illustrating a triple step voltage routine that enables ~10 ms piezo movement with minimal vibration. See online methods for further details.

Supplementary Fig. 7, Immunolabeled microtubules viewed by instant SIM

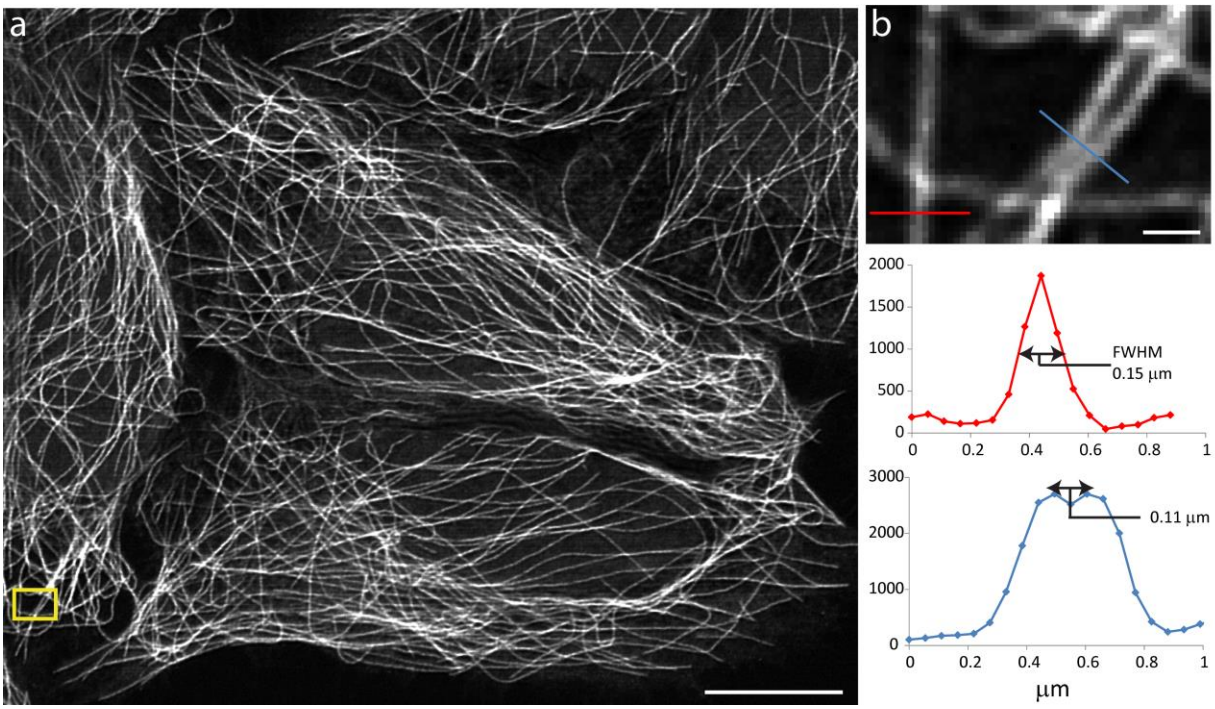

(a) Maximum intensity projection of Alexa Fluor 488 antibody labeled microtubules in a U2OS cell, after analog processing shown in **Fig. 1** and deconvolution. Scalebar: 10 µm. **(b)** Top panel: Higher magnification view of the yellow boxed region in **(a)**; Middle and bottom panels indicate apparent microtubule width and separation, corresponding to the red and blue lines marked in top panel. Scalebar: 500 nm.

Supplementary Fig. 8, Cross-sectional lineouts of 100 nm yellow green beads, as viewed in line-scanning, spinning-disk confocal, and instant SIM systems.

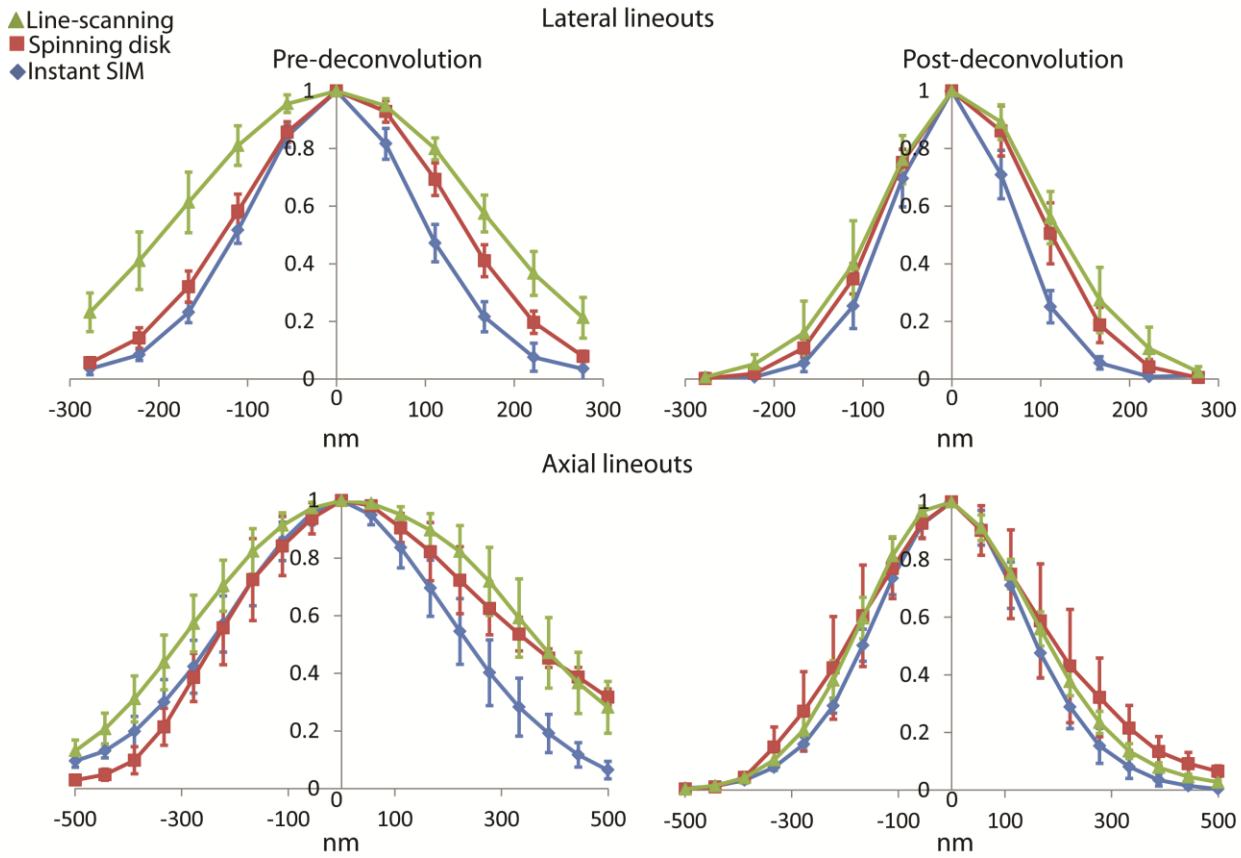

Lateral (top) and axial (right) lineouts through 5 yellow green 100 nm fluorescent beads, pre-(left column) and post-(right column) deconvolution. Beads always appear sharpest in instant SIM. See also **Table 1, Fig. 2,** and **Supplementary Fig. 9**.

Supplementary Fig. 9, Apparent size of subdiffractive beads as viewed in line-scanning, spinning-disk confocal, and instant SIM systems.

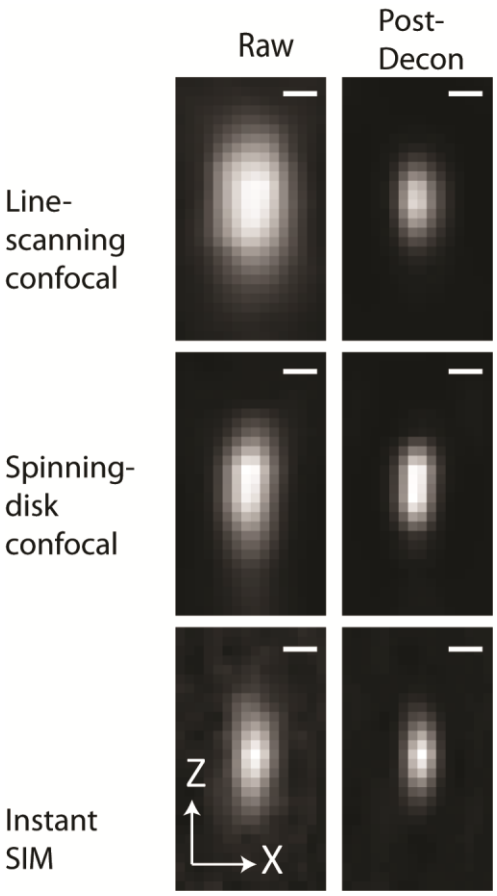

XZ cross-sectional views of 100 nm yellow-green fluorescent beads before (left column) and after (right column) deconvolution. See also **Supplementary Fig. 8** and **Table 1.** Scalebars: 200 nm.

Supplementary Fig. 10, Voids in mitochondria, as revealed by instant SIM.

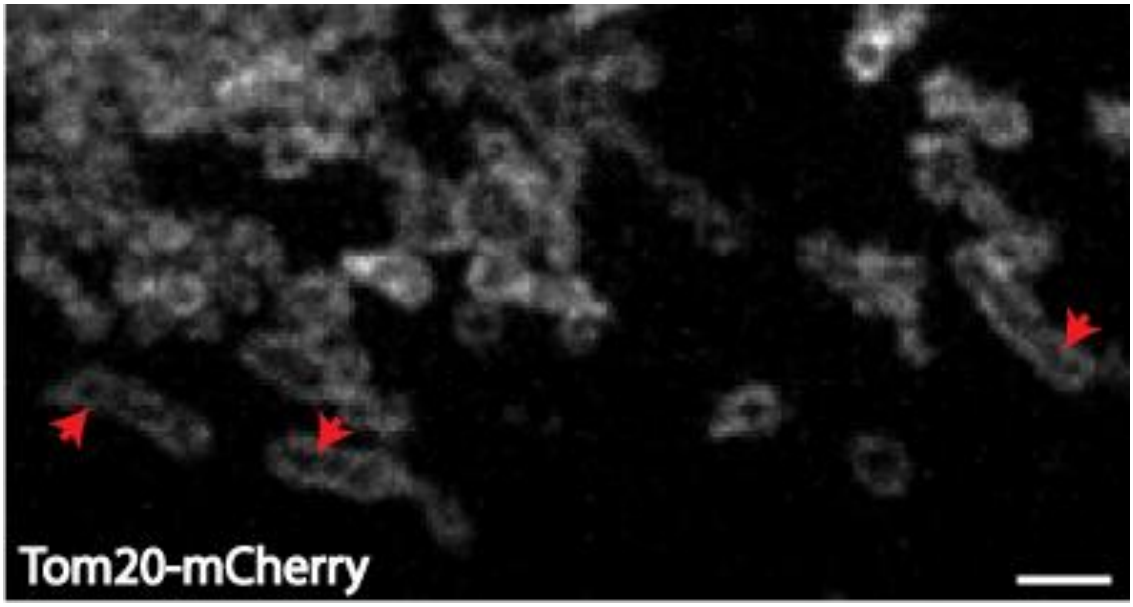

Higher magnification view of a subregion of the Tom20-mCherry image in **Fig. 2**. Red arrows mark the inner mitochondrial space (voids). Scalebar: 1 μm.

Supplementary Fig. 11, Mitochondria visualized in line-scanning, spinning disk confocal, and instant SIM systems, without deconvolution.

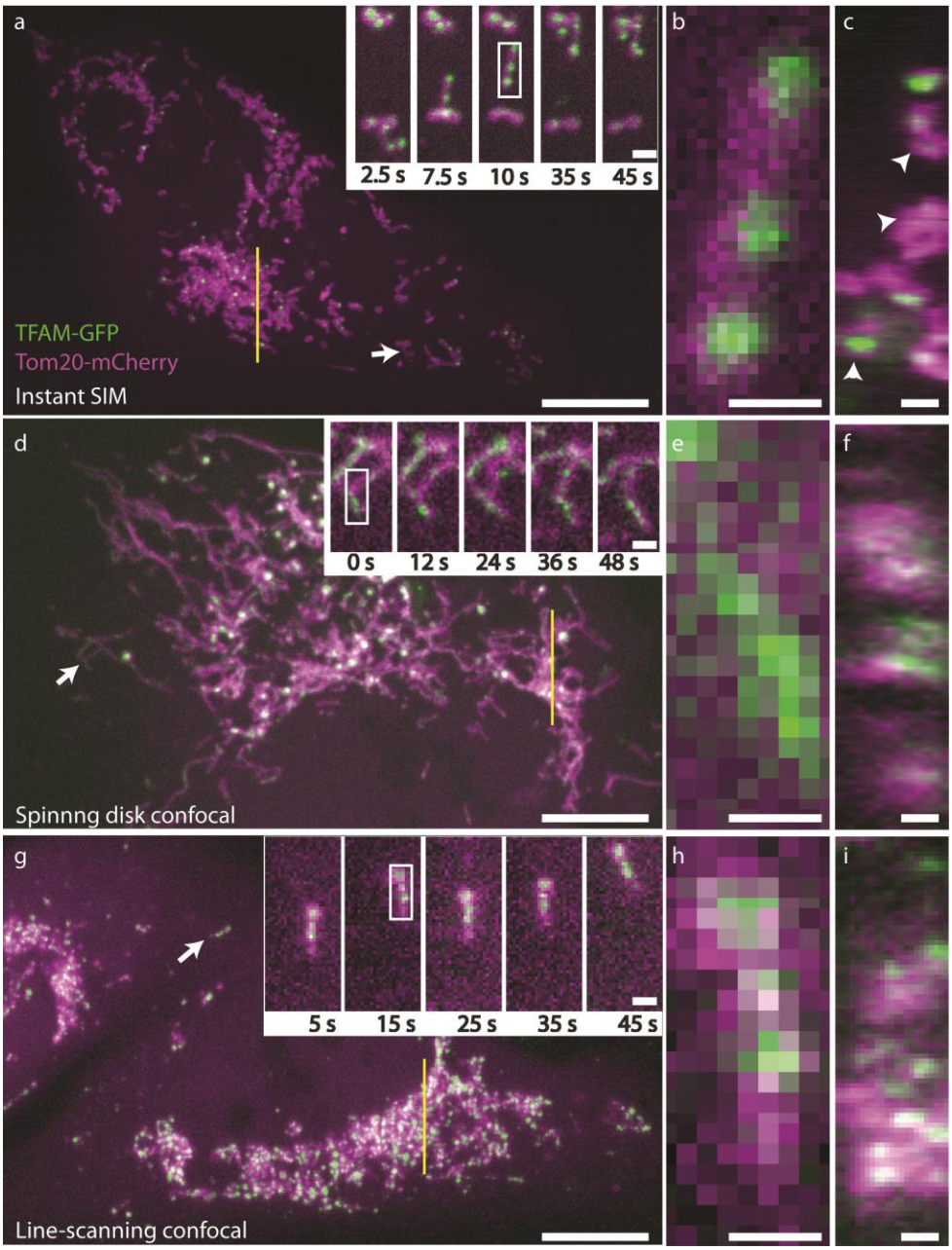

Live MRL-TR transformed human lung fibroblasts expressing TFAM-GFP (green) and Tom20-mCherry (red) were imaged in instant SIM (**a-c**), a spinning disk confocal microscope (**d-f**), and a line scanning confocal microscope (**g-h**). Data and annotations are identical to those in **Fig. 2**, but data has not been deconvolved. Instant SIM achieves better resolution than either spinning disk or line-scanning confocal microscopy.

Supplementary Fig. 12, Deconvolution improves spinning disk and line-scanning confocal resolution, but not to the extent offered by instant SIM.

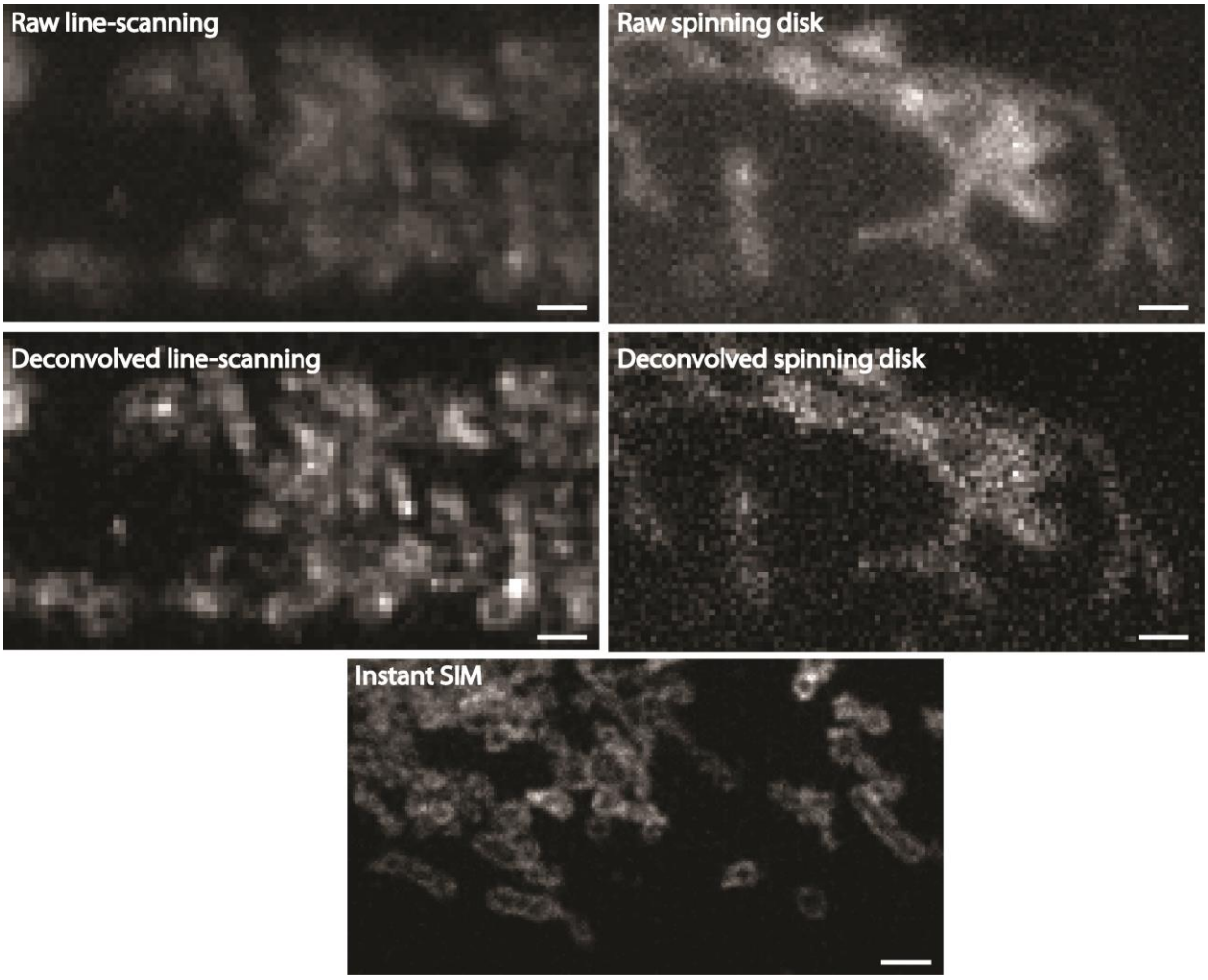

Tom20-mCherry images were acquired with a line-scanning confocal microscope (left), a spinning disk confocal microscope (right), and instant SIM (bottom). Unlike instant SIM, sub-mitochondrial features are not resolved in either line-scanning or spinning disk microscopes, even after deconvolution (right column). Scalebars: 1 μm.

Supplementary Fig. 13, Axial sectioning of different microscopes

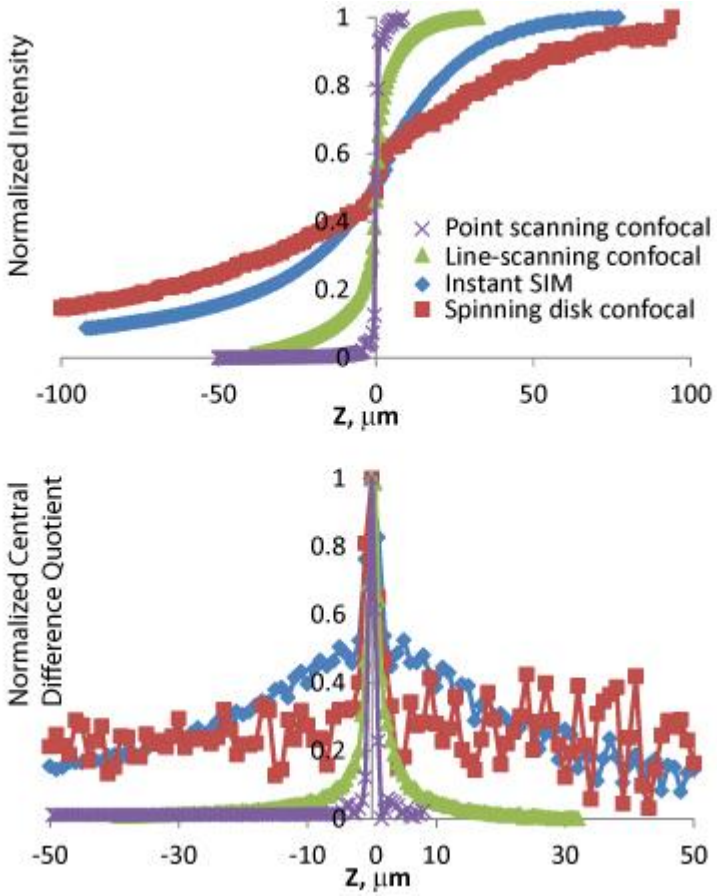

Point-scanning (LSM 510), line-scanning, spinning disk, and instant SIM systems were used to image a thick fluorescent lake. Top: axial response as a function of defocus, bottom: central difference quotient (approximate derivative) of the same data. Instant SIM gives similar sectioning to spinning disk confocal, and worse sectioning than line- or point-scanning confocal techniques.

Supplementary Table 1, Primer sequences

Name	Sequence
SEC61A Forw	ACAGTCGACATGGCAATCAAATTTCTG
SEC61A Rev	ATAGGTACCTTAGAAGAGCAGGGCCCCC
Tom20 Forw	CACAGATCTATGGTGGGTCGGAACAGCGC
Tom20 Rev	ATAGAGCTCTTCCACATCATCTTCAGCC
TFAM Forw	CACAGATCTATGGCGCTGTTCCGGGGAAT
TFAM Rev	ATAGAGCTCATGCTCAGAGATGTCTCCGG

See online methods, 'Molecular biology and cloning procedures' for accompanying context.

Supplementary Note 1, Explanation of resolution-doubling in instant SIM.

To understand the mechanism of resolution doubling in instant SIM, it is helpful to first understand the mechanism of resolution doubling in a standard point-scanning confocal microscope. A point-scanning confocal microscope with a pinhole closed almost completely produces a point-spread function (PSF) that is 1.4x narrower in the lateral direction, and doubles the frequency content of the resulting image[1]. To illustrate the mechanism in more detail, we examine simulated images of test objects.

Fig. S1 shows a cross section of three idealized test objects. The x-direction points left-right, the y-direction points into and out of the page, and the z-direction points up-down along the page. Test objects are invariant in the y-direction. The left test object is a thin line, like a microtubule. The middle test object is a cylindrical shell with two septa dividing it into quadrants. The right test object is a set of parallel sheets with variable spacing, oriented in the xy and xz planes.

Fig. S1, Idealized test objects used in simulations

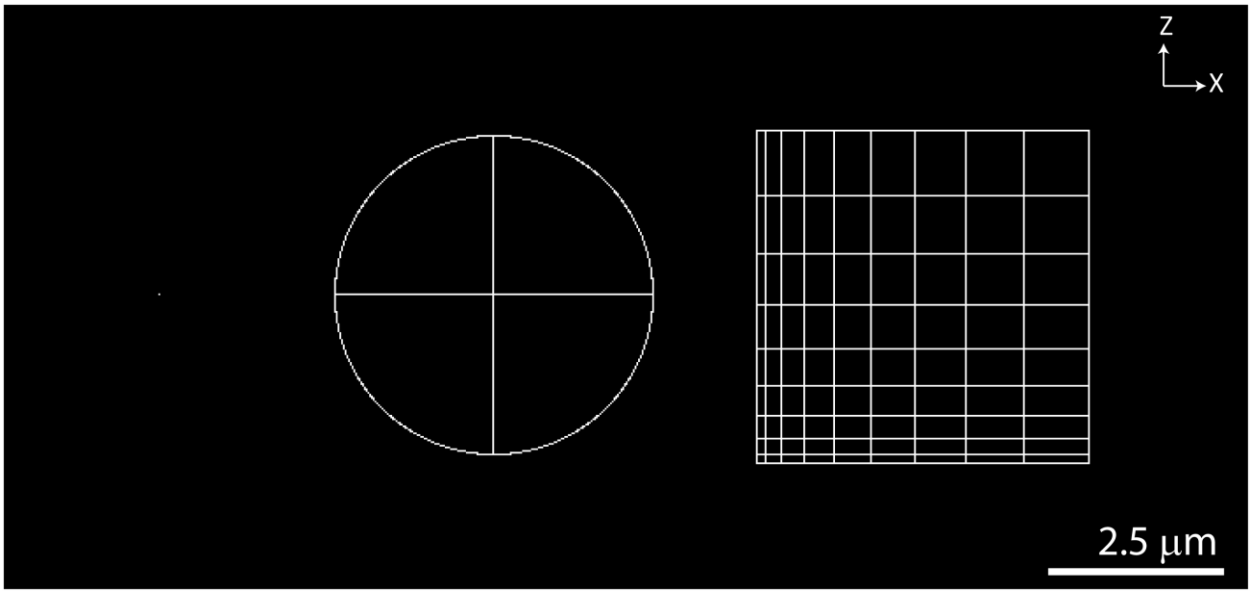

Fig. S2 shows these test objects viewed with a confocal microscope. The test object is blurred with a calculated point spread function (PSF) using three different pinhole sizes. PSFs were calculated using the PSF Generator ImageJ plugin, available at http://bigwww.epfl.ch/algorithms/psfgenerator/#bw, with NA 1.4, index 1.5, wavelength 500, and pixel size 25 nm.

Fig. S2, Test objects viewed through a confocal microscope

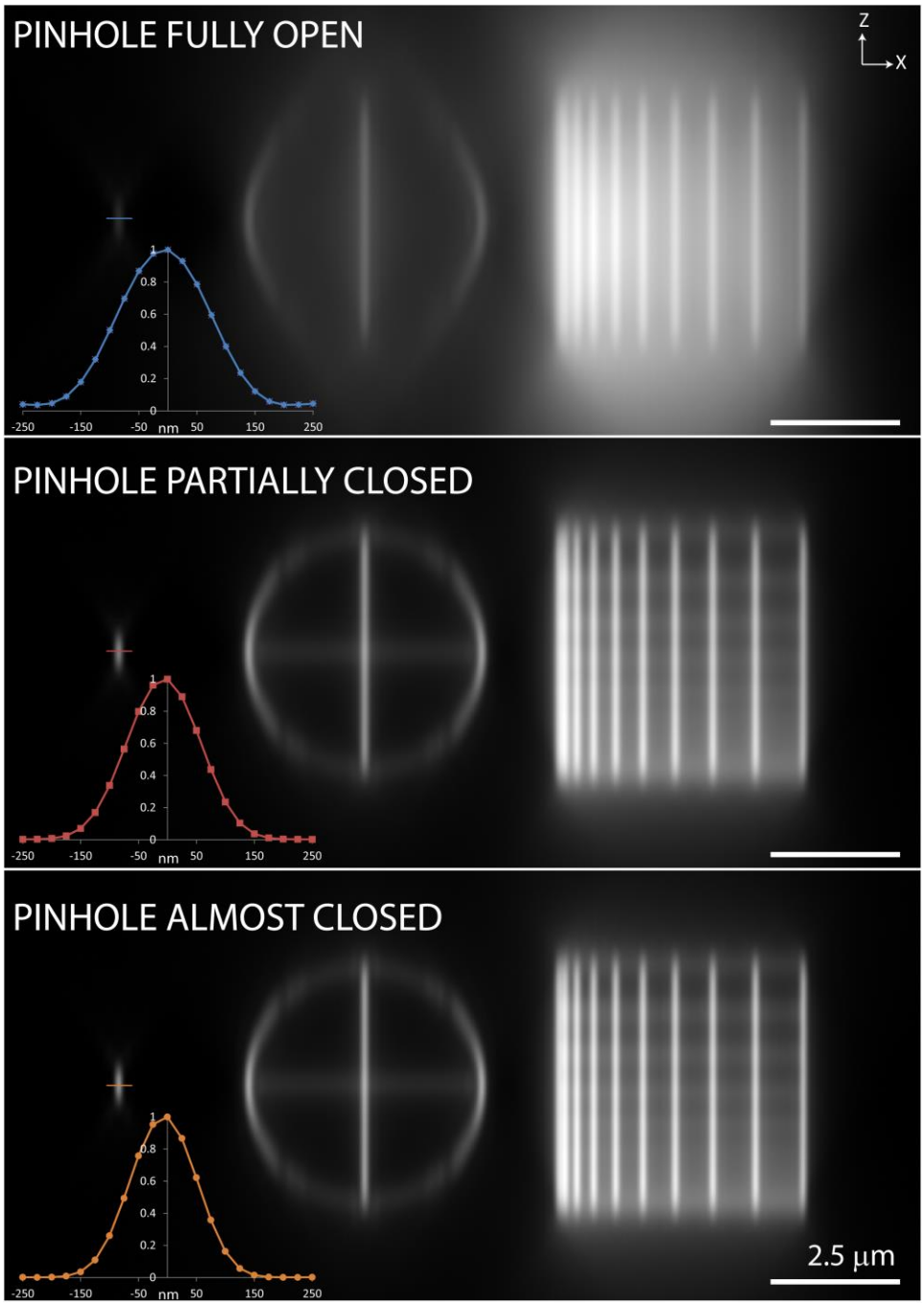

The top panel of **Fig. S2** shows an image taken with a fully-open pinhole. In this case, the microscope's PSF is determined simply by the excitation PSF, the shape of the focused excitation laser beam. Lateral features (shown by the width of the line-like test object in the inset) are reasonably resolved, but axial structure of the sheets oriented in the xy-plane is almost completely obscured. Axial features are poorly imaged because the excitation laser beam does not die off in the axial direction, it merely spreads out.

The middle panel of **Fig. S2** shows an image taken with a partially-closed pinhole (225 nm diameter in the image plane). In this case, the microscope's PSF is the product of its excitation and emission PSFs, and the emission PSF is the convolution of the widefield emission PSF with the partially open pinhole. Convolution with the partially-open pinhole further blurs the widefield emission PSF, but the product of this blurred emission PSF with the excitation PSF is still narrower than the excitation PSF alone. Additionally, the product of the excitation and emission PSFs dies off in the axial direction, so thin sheets oriented in the xy plane are now visible. Because the transverse resolution is improved in this configuration due to the combination of excitation and emission PSFs, confocal microscopy with a partially closed pinhole can be regarded as a form of structured illumination microscopy, albeit without fully doubled resolution compared to widefield microscopy.

The bottom panel of **Fig. S2** shows an image taken with a pinhole that is almost completely closed (25 nm diameter in the image plane). As in the middle panel, the microscope's PSF is the product of the excitation and emission PSFs, but now the emission PSF is not blurred by convolution with a large pinhole. Since the excitation and emission PSFs are nearly equal for most fluorescence microscopes, the resulting PSF is effectively the square of the widefield PSF, improving resolution by $\sqrt{2}$. Since multiplication in the spatial domain is equivalent to convolution in the spectral domain, it is clear that the frequency content of this microscope's image is doubled, implying that deconvolution can improve spatial resolution a full factor of two compared to widefield microscopy.

However, this doubled resolution is usually not useful in practice. **Fig. S3** shows simulated relative noise levels for the same images shown in **Fig. S2**. Assuming an ideal detector with no noise, measured signals still contain Poisson noise, and the signal-to-noise ratio (SNR) scales as the square root of the signal. The top panel of **Fig. S3** shows a very bright widefield signal, difficult to distinguish from the noise-free case. In the middle panel, the test object is the same brightness as the top panel, but the partially-closed confocal pinhole rejects a substantial portion of the emission light. Noise is noticeable in this image, but the resolution is still much better than in the widefield case. In the bottom panel, the fully-closed pinhole rejects far too much of the emission light; any improvement in resolution compared to the middle panel is masked by the severe degradation in SNR.

Fig. S3, The influence of noise when imaging with a pinhole

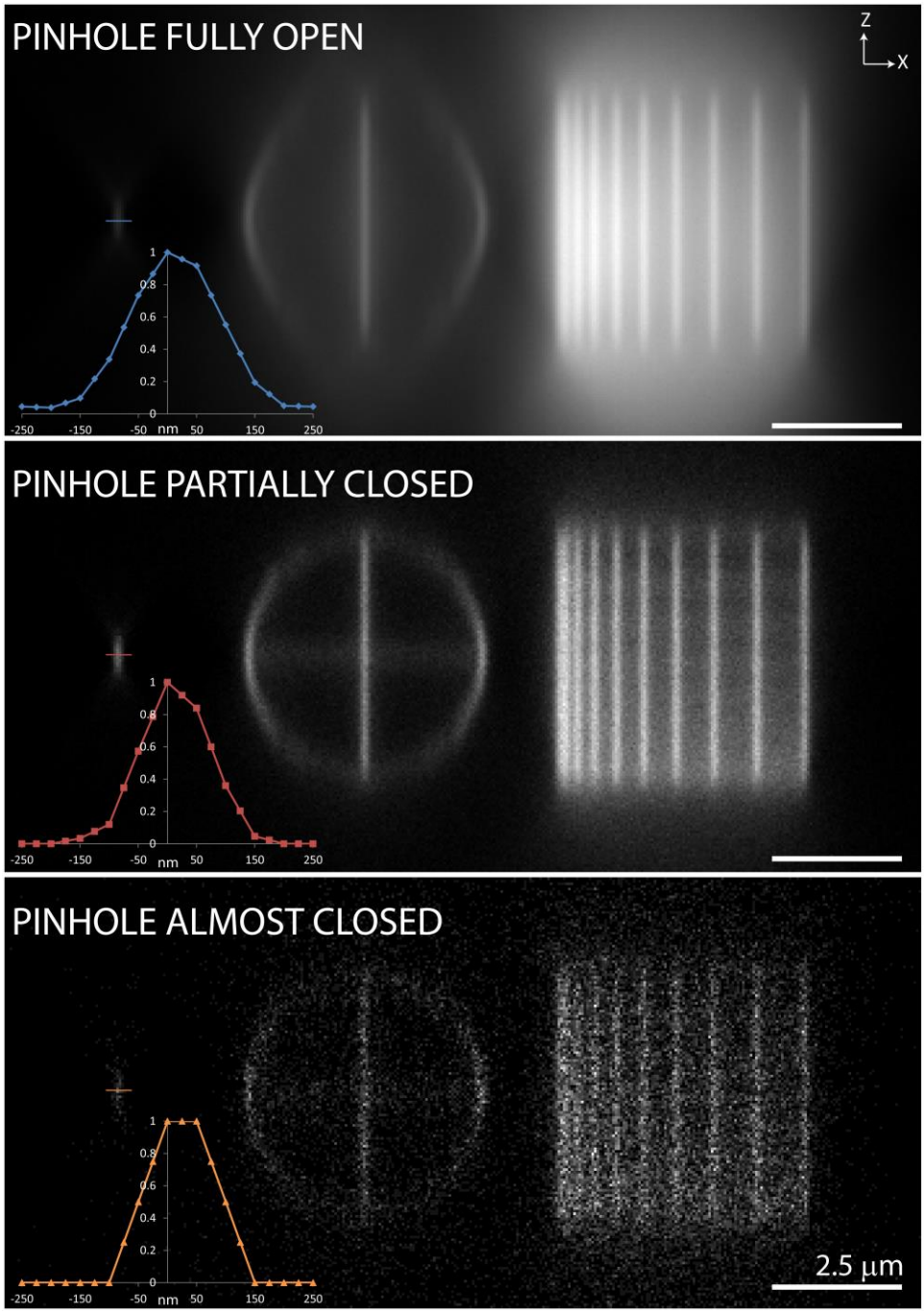

Ref.[1] suggests a method for improving resolution without sacrificing signal: close the pinhole nearly all the way, but use multiple nearly-closed pinholes to collect and combine the majority of the emission light. However, a naive summing of images will not work, as lateral misalignment alters the collected image. The top panel of **Fig. S4** shows one such image, collected with a laterally displaced pinhole (150 nm effective displacement to the left in the image plane). Superficial features of the image are similar to the bottom panel of **Fig. S2**, but the

image is even dimmer, and more importantly, the image is laterally shifted. A second image collected with a second pinhole shifted in the opposite direction (150 nm effective displacement to the right in the image plane) produces a similar image, but shifted in the opposite direction. Simply adding these two images, as shown in the bottom panel of **Fig. S4**, produces a 'doubled' image, with substantially worse resolution than the individual images.

Fig. S4, The result of laterally shifting the pinholes

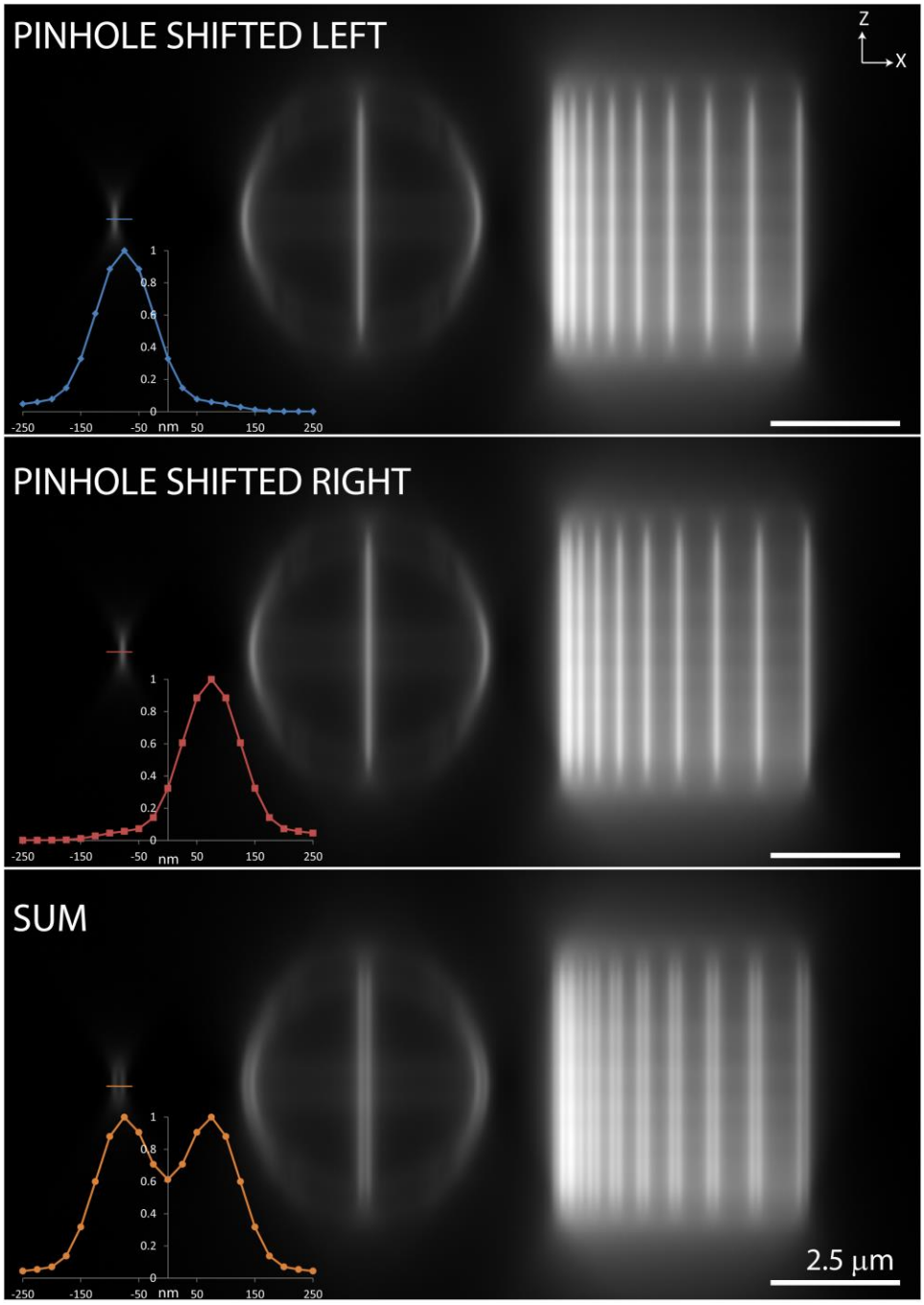

Combining additional nearly-closed pinholes does not solve the problem; the top panel of **Fig. S5** shows the result of adding the images collected by several small pinholes. The double-image is eliminated, but resolution is not improved compared to the partially-closed pinhole shown in the middle panel of **Fig. S2**. However, there is an alternative method for eliminating the double-image: simply shift the individual images appropriately before summing them! The bottom panel of **Fig. S5** is a sum of the same images used to construct the top panel, but each image has been shifted before summing. As expected[1,2], the appropriate shift amount is half the amount that the pinhole is displaced, and the appropriate shift direction is opposite to the direction that the pinhole was displaced. For example, the 150 nm pinhole displacements used in **Fig. S4** collect images that must be shifted 75 nm before summing with an image from an undisplaced pinhole.

Fig. S5, Summing, then shifting pinholed images improves resolution without sacrificing signal

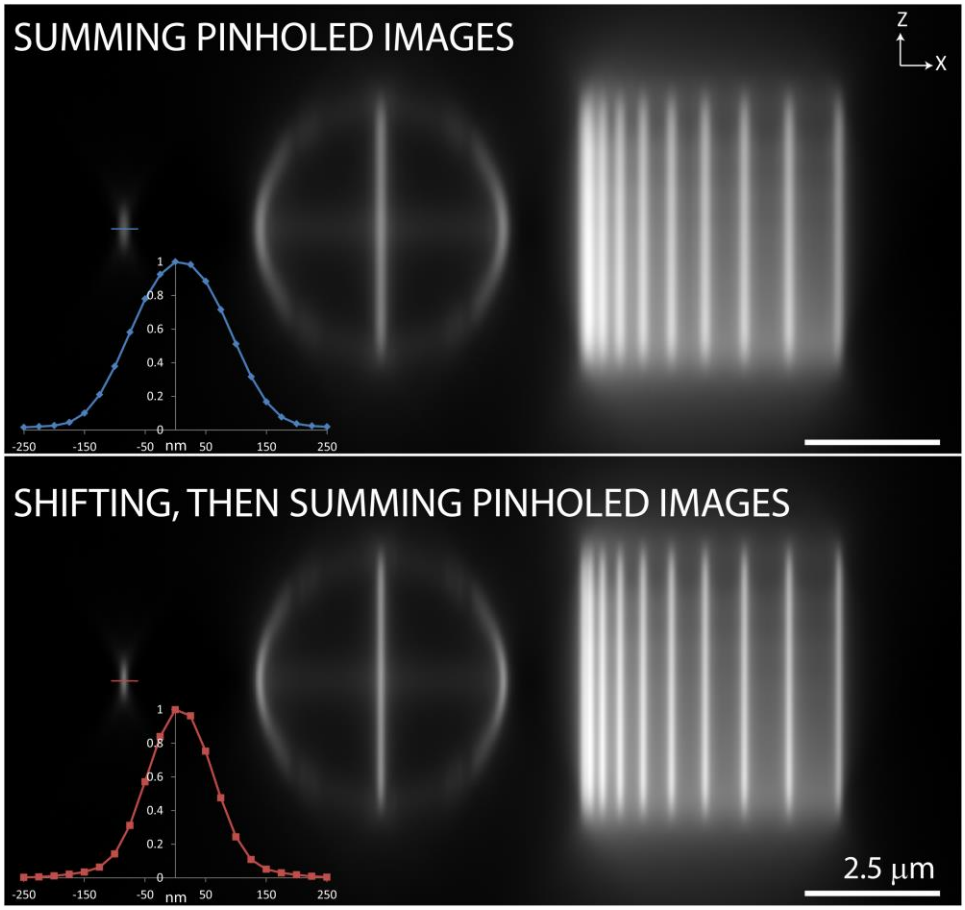

The key principle which allows resolution doubling in a confocal point-scanning microscope without sacrificing signal is thus to use multiple small pinholes, but shift the images appropriately in order to compensate for the shift induced by pinhole misalignment before summing their signals. In previous digital implementations such as image scanning microscopy

(ISM)[2] or multifocal structured illumination microscopy (MSIM)[3], shifting is accomplished computationally. In instant SIM, shifting is accomplished optically. As shown in the top panel of **Fig. S6**, this splits the job of the confocal pinhole between two separate types of pinhole, "micropinholes", and the "macropinhole".

Figure S6, Macro- and micropinholes in instant SIM

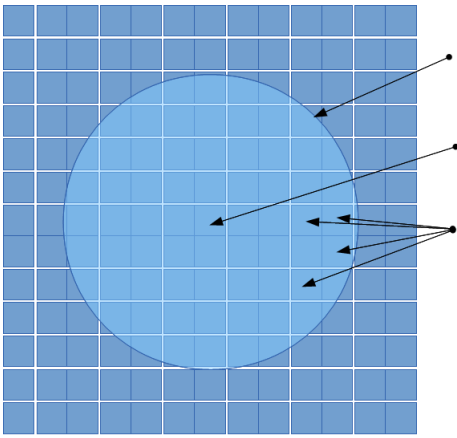

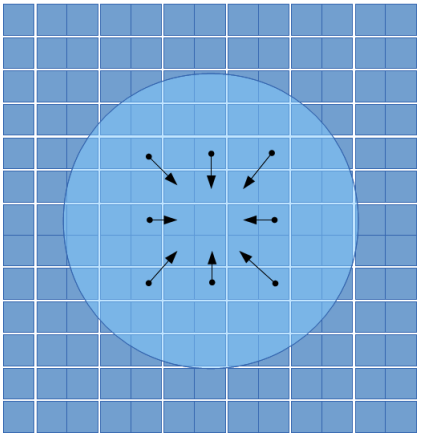

The macropinhole plays the same role as the partially-closed pinhole used for the middle panel of **Fig. S2-S3:** it rejects out-of-focus light to provide optical sectioning, but is not small enough to double transverse resolution, or to badly degrade signal levels. In MSIM, the macropinhole was applied with digital postprocessing; in ISM and instant SIM, the macropinhole is implemented optically with a physical pinhole.

The micropinholes play the role of the nearly-closed pinhole, allowing doubled transverse resolution. As shown in the top panel of **Fig. S6**, the micropinholes are not centered, so their individual images must be corrected. In ISM, MSIM, and instant SIM, the pixels of the camera detector are used as micropinholes. In ISM and MSIM, the correction is implemented by collecting multiple exposures with different illumination positions, and digitally reassigning the collected signal to different image bins using interpolation. The reassignment is simple: since a pinhole displaced by X collects an image displaced by X/2, shrink the image of each pinhole by a

factor of 2 towards the center of the pinhole. In instant SIM, this correction is implemented by using a microlens to 'shrink' pinholed images by a factor of 2 before they reach the detection camera; no interpolation is required, due to the analog nature of reality. Note that these two approaches, digital and analog, are entirely equivalent, except that the analog approach is much faster.

With this understanding of how a single illumination point at a particular sample position contributes signal to the image, we construct the full super-resolution image by scanning the illumination over the entire sample. In ISM, a single excitation point is used, providing excellent sectioning but slow speed. The camera is placed in the descanned emission path, so micropinholes are stationary with respect to the macropinhole and the required shift, applied digitally, is independent of scan position. In MSIM, multiple excitation points are used to increase acquisition speed, albeit at the cost of pinhole crosstalk. In MSIM the emission is not descanned, so micropinholes are not stationary with respect to the macropinhole. The required shift, implemented digitally, changes with scan position. Instant SIM, like MSIM, uses multiple excitation points to speed acquisition. Like ISM, the emission is descanned, so the required shift is independent of scan position, but the shifting is performed optically (with a microlens array), rather than digitally. Following the shifting, the beam is rescanned to produce a stationary image of the sample on the camera, as in MSIM. In all implementations, as long as the sample is 'painted' evenly, the resulting image appears smooth. We note that our implementation of instant SIM has several 'dead' microlenses, resulting in a striping artifact in portions of our images. We anticipate that better quality control would solve this problem.

Noise levels, of course, are crucial to image quality and resolution. ISM uses a moderate number of optics in the emission path, but a very small scan step size. This provides reasonable transmission efficiency (preventing excess Poisson noise), but requires many exposures (and thus an increased level of read noise). MSIM uses fewer emission optics and a larger step size than ISM, improving both Poisson and read noise, although presumably provides worse sectioning than ISM due to pinhole crosstalk. Instant SIM has more emission optics than ISM, but uses only a single camera exposure, thus increasing Poisson noise but minimizing read noise. Finally, we note that digital macropinholes compared to analog macropinholes give approximately equivalent levels of background rejection; emission light that falls outside the macropinhole is ignored in either case.

We note that if excitation and emission PSFs are not so nearly identical (as in two-photon microscopy or stimulated emission depletion microscopy, for example), the appropriate amount to shrink the image of the pinhole is no longer a factor of 2; smaller excitation PSFs demand more shrinking, and larger excitation PSFs demand less shrinking, assuming the emission PSF stays the same size. The appropriate shift can be estimated precisely by calculating the position of the maximum of the product of the excitation PSF with the shifted emission PSF.

1 Sheppard, C. J. R. Super-resolution in Confocal Imaging. *Optik* **80**, 53-54 (1988).
2 Muller, C. B. & Enderlein, J. Image Scanning Microscopy. *Physical Review Letters* **104**, 198101 (2010).
3 York, A. G. *et al.* Resolution Doubling in Live, Multicellular Organisms via Multifocal Structured Illumination Microscopy. *Nature Methods* **9**, 749-754 (2012).